

# The Enhanced Tribological Properties of NiAl Intermetallics: Combined Lubrication of Multilayer Graphene and WS<sub>2</sub>

Jie Yao · Xiaoliang Shi · Wenzheng Zhai · Ahmed Mohamed Mahmoud Ibrahim · Zengshi Xu · Long Chen · Qingshuai Zhu · Yecheng Xiao · Qiaoxin Zhang · Zhihai Wang

Received: 26 May 2014 / Accepted: 13 October 2014 / Published online: 21 October 2014  
© Springer Science+Business Media New York 2014

**Abstract** In recent years, reducing friction and wear-related adverse impacts on efficiency and durability in moving mechanical systems has gained increased attention. Herein, the search continues for novel materials and lubricants that can potentially reduce friction and wear. As one of the emerging self-lubricating materials, the tribological potential of graphene has been researched deeply. This article was dedicated to explore the combined lubrication of multilayer graphene (MLG) and WS<sub>2</sub>. The as-prepared sample of NiAl–1.5 wt% MLG–5 wt% WS<sub>2</sub> (NB) exhibited excellent tribological properties. During the sliding process, a continuous lubricating film was formed to provide the low-strength junctions at the interface, reducing the friction coefficient and wear rate. Moreover, the MLG played the role of reinforcement particles and improved loading carrying ability.

**Keywords** Self lubrication friction · Self-lubricating composites · Solid lubricants · Solid lubrication mechanisms · Solid lubrication wear

## 1 Introduction

The rapid development of industry and scientific technology requests materials and structures to work under extreme environment conditions, i.e., high-temperature, high-pressure and vacuum conditions where the most

traditional metals cannot meet the requirement of friction applications. Herein, liquid lubricants fail to work effectively, and coatings have limited service life. By contrast, metal matrix self-lubricating composites (MMC) which have excellent tribological performance and a longer life-span due to the self-repair capability are good alternative when lubrication, friction and wear are the limiting factors [1]. During dry sliding process, lubricating films formed on the worn surfaces of the self-lubricating composites, significantly reduce the friction and wear [2, 3]. As a kind of high-performance structural materials as well as functional materials with a great application potential in special conditions, MMC that consist of different metallic matrixes and different solid lubricants have been extensively investigated by the engineers and researchers in the field of tribology in recent decades [4–7].

NiAl intermetallics can be used as ideal structural materials due to their superior performance of high melting point (1,638 °C), low density (5.95 g cm<sup>-3</sup>), high Young's modulus (294 GPa), high thermal conductivity (70 Wm<sup>-1</sup> K<sup>-1</sup>) and excellent oxidation resistance [8, 9]. However, the tribological properties need to be characterized for NiAl intermetallics as the candidate for structural components. The dry sliding wear behavior of NiAl intermetallic against zirconia further indicated that NiAl intermetallic was a desirable matrix for the preparation of self-lubricating composites in moving mechanical systems [10, 11]. Accordingly, studies have been carried out in recent years to investigate the tribological properties of NiAl matrix self-lubricating composites (NASC) [12–14]. The researches show that NiAl intermetallic is a desirable matrix to design NASC, which possess superior tribological properties, and the choice of solid lubricants is very important.

As one of the emerging self-lubricating materials, the multilayer graphene (MLG) has attracted tremendous

J. Yao · X. Shi (✉) · W. Zhai · A. M. M. Ibrahim · Z. Xu · L. Chen · Q. Zhu · Y. Xiao · Q. Zhang · Z. Wang  
School of Mechanical and Electronic Engineering, Wuhan University of Technology, 122 Luoshi Road, Wuhan 430070, China  
e-mail: sx1071932@126.com; sx1@whut.edu.cn

attention. The previous studies demonstrate that graphene has excellent mechanical properties with a high Young's modulus of 1TPa and high fracture strength of 130 GPa [15]. However, compared with the works on general properties of graphene, the tribological applications are still the least explored. Lin et al. [16] studied friction and wear characteristics of MLG films investigated by atomic force microscopy. It was found that graphene films exhibited much lower friction than bare Si surface. Kvetkova et al. [17] prepared graphene platelet-reinforced  $\text{Si}_3\text{N}_4$  composite containing 1 wt% graphene using hot isostatic pressing and reported an increase of about 44 % in fracture toughness over the pure  $\text{Si}_3\text{N}_4$ . Xu et al. [18] reported on preparation and tribological properties of TiAl matrix composites reinforced by MLG. The research showed that MLG could act as an effective reinforcing and lubricating phase, reducing the friction coefficients and wear rates of TiAl matrix composites. Therefore, graphene can be used as a high-performance solid lubricant. While due to the folding structure and low density, large mass fraction of MLG will reduce the physical mechanical properties of composites [19]. Moreover, Kandamur et al. [20] demonstrated that MLG could reduce the wear of other solid lubricants when as nano-fillers. MLG was able to interfere with the formation of cracks and provide easy shear force, thus enhancing the bond between matrix and lubricants. Hence, an unexpected lubricating effect can be obtained as MLG, and other solid lubricants are combined utilization, overcoming disadvantage of the single lubricant.

Transition metal dichalcogenides such as  $\text{MoS}_2$  and  $\text{WS}_2$  are widely used for solid lubricants due to their extreme degree of anisotropy of the layered crystal structures. They are characterized by weak interatomic interactions between their layered structures and easy to be sheared, forming transfer lubricious film between the friction pair interface. The basic structure and performance of  $\text{WS}_2$  are similar to the well-researched  $\text{MoS}_2$  [21]. In addition,  $\text{WS}_2$  has relatively high oxidation temperature (539 °C) than  $\text{MoS}_2$  (370 °C) or graphite (325 °C), so it can maintain lubricating property at relatively higher temperature [22].

MLG and  $\text{WS}_2$  are both laminar structure and easy to be sheared, forming transfer lubricious film on the worn surface. The mixtures of MLG and  $\text{WS}_2$  may have advantages and overcome disadvantages of single lubricant, providing an effective synergistic lubrication by forming lubricating film.

According to our experience in the past, 1.5 wt% MLG and 5 wt%  $\text{WS}_2$  are reasonable to improve the tribological properties of metal-based composite [23, 24]. In this article, 1.5 wt% MLG and 5 wt%  $\text{WS}_2$  are used as combined lubricants to design NASC. This method is able to get

excellent tribological properties without causing degradation of the physical mechanical properties. Tribological behaviors of the as-prepared composites are investigated by sliding against a 6-mm-diameter ball made of  $\text{Al}_2\text{O}_3$ ,  $\text{Si}_3\text{N}_4$  and WC–6Co. NiAl composite without MLG and  $\text{WS}_2$  is also prepared and tested under the same conditions for the purpose of comparison. Present work is expected to ascertain whether MLG and  $\text{WS}_2$  can have an effective synergistic lubrication, and provide a clue for the design of self-lubricating composites.

## 2 Experimental Details

### 2.1 Materials

NiAl composite (NA) and NiAl matrix self-lubricating composite with 1.5 wt% MLG and 5 wt%  $\text{WS}_2$  (NB) were prepared through the spark plasma sintering (SPS) at a temperature of 1,100 °C and a pressure of 35 MPa for 10 min in pure Ar atmosphere protection. The composite powders of NiAl matrix were composed of commercially available Ni, Al, Mo and Nb powders (30–50  $\mu\text{m}$  in average size, 99.9 wt% in purity) by atomic ratio of 48:50:1:1. MLG and  $\text{WS}_2$  powders were purchased from Nanjing XFNANO Materials Tech Co., Ltd. The MLG produced by chemical mechanical stripping method had an average thickness of 40 nm and an average lateral dimension of 50  $\mu\text{m}$ . The average grain size of  $\text{WS}_2$  powders was about 20–40  $\mu\text{m}$ . The as-prepared specimen surfaces were ground to remove the surface layer and polished mechanically with emery papers down to 1,200 grit, and then with 0.05  $\mu\text{m}$  wet polishing diamond pastes up to a mirror finish.

The Vicker's microhardness of each as-produced sample was measured by using a HVS-1000 Vicker's hardness instrument with a load of 1 kg and a dwell time of 8 s according to the ASTM Standards E384-11e1 [25]. Ten tests were conducted, and the mean value and standard deviation were given. Meanwhile, the measured density was determined by Archimedes' principle according to the ASTM Standards B962-13 [26]. Ten tests were conducted, and the mean value and standard deviation were given.

### 2.2 Tribological Test

The dry friction and wear tests were carried out on a HT-1000 ball-on-disk high-temperature tribometer (made in Zhong Ke Kai Hua Corporation, China) according to the ASTM Standards G99-05 [27]. The disk, which was the as-prepared sample, rotated with a constant speed. The counterface balls were commercially available balls of WC–6Co (16.0 GPa),  $\text{Si}_3\text{N}_4$  (15.0 GPa) and  $\text{Al}_2\text{O}_3$

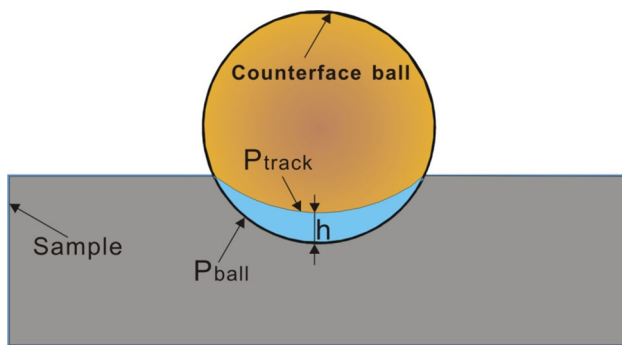


**Fig. 1** Comparison of theoretical profile ( $P_{\text{ball}}$ ) across a 6-mm-diameter ball and measured profile ( $P_{\text{track}}$ ) across the wear track on the sample

(18.0 GPa), which were polished to an average surface roughness ( $R_a$ ) of 0.01  $\mu\text{m}$ . The disks and counterface balls were cleaned by acetone solution and then dried in hot air before frictional wear tests. The friction coefficient was automatically measured and recorded in real time by the computer system of the friction tester. The wear rate was calculated by the following formula  $W = V/SF_N$ , where  $V$  was the wear volume,  $S$  was the sliding distance and  $F_N$  was the normal load. Wear volume of the samples was determined by measuring the cross-sections of the wear track with a stylus profilometer. While the stylus was moving across the wear track, the vertical and horizontal positions of the stylus were recorded and later processed using Microsoft Excel, so that a 2D profile of the wear track was obtained. The wear volume  $V$  was calculated using the equation  $V = AL$ , where  $A$  was the cross-section area of the worn scar and  $L$  was the perimeter of the wear track [28]. The tests for every given conditions were repeated three times to obtain reliable data. The average value was used as the evaluating data.

Wear volume of the counterface ball was achieved by comparing the wear track profile ( $P_{\text{track}}$ ) on the sample with the theoretical profile of a 6-mm-diameter ball ( $P_{\text{ball}}$ ) as shown in Fig. 1. The track profile  $P_{\text{track}}$  was measured with a stylus profilometer across the wear track after tests. The profile across the ball ( $P_{\text{ball}}$ ) was theoretically calculated according to the equation of  $y^2 = r^2 - x^2$ , where  $r = 3$  mm was the radius of the counterface ball,  $y$  and  $x$  were coordinators of a point in the circular profile. Assuming that the counterface ball had a close contact with the wear track on the sample, then the shadowed area between the profiles of  $P_{\text{track}}$  and  $P_{\text{ball}}$  would represent materials on the counterface ball, which had been worn away during sliding test. Quantification of ball wear volume was proven to be difficult, but semi-quantity calculation was possible for a comparison purpose [28]. The maximum ball worn height,  $h$ , representing the linear

dimension loss could be used to evaluate the wear performance of a counterface ball. Hence, the wear volume  $V$  of the counterface ball could be approximately calculated using the equation of  $V = \pi h^2(r - h/3)$ . The tests for every given conditions were repeated three times to obtain reliable data. The average value was used as the evaluating data.

### 2.3 Microstructure Analysis

The surfaces of the as-prepared specimens were examined by XRD with Cu  $K\alpha$  radiation at 30 kV and 40 mA at a scanning speed of 0.01  $\text{s}^{-1}$  for the identification of the phase constitution and Raman spectroscopy (RENISHAW, INVIA). The worn surfaces of as-prepared composites were characterized using electron probe microanalyzer (EPMA, JAX-8230) and energy dispersive spectroscopy (EDS, Inca X-Act). The morphologies and compositions of cross-sections of worn surfaces of TB obtained when sliding against  $\text{Si}_3\text{N}_4$  were analyzed by a field-emission scanning electron microscope (FESEM, FEI-SIRION). In order to investigate the phase distribution of subsurface under the worn surface, the cross-section of worn surface of TB obtained when sliding against  $\text{Si}_3\text{N}_4$  was carefully polished with emery papers down to 2,000 grit and then with 0.05  $\mu\text{m}$  wet polishing diamond pastes. Then, the cross-section was handled by vibration polishing with an alumina suspension (Buehler VibroMet<sup>®</sup> 2 Vibratory Polisher), ultrasonic washing with anhydrous ethanol and then drying in vacuum at room temperature for 0.5 h. The electron backscatter diffraction (EBSD) of subsurface under the worn surface of NB obtained when sliding against  $\text{Si}_3\text{N}_4$  was undertaken on a Nordlys EBSD detector with a Peltier cooled CCD camera and operating at 20 kV with an acquisition speed of 288.16 Hz.

## 3 Results and Discussion

### 3.1 Compositions and Hardness of Composites

Figure 2 shows the XRD patterns of NA and NB. As shown in Fig. 2, the diffraction peaks in NA primarily belong to NiAl phase, and the diffraction peaks in NB belong to NiAl,  $\text{WS}_2$  and C phases. It reveals that Ni powder and Al powder have gone through synthesis reactions to form NiAl phase, and  $\text{WS}_2$  and MLG do not react with Ni and Al, thereby eliminating any reaction products at the interface between the additives and the matrix. In order to verify MLG still being retained in NB after SPS, the Raman spectra of NB are shown in Fig. 3. It exhibits three main characteristic peaks: the G mode, a doubly degenerate

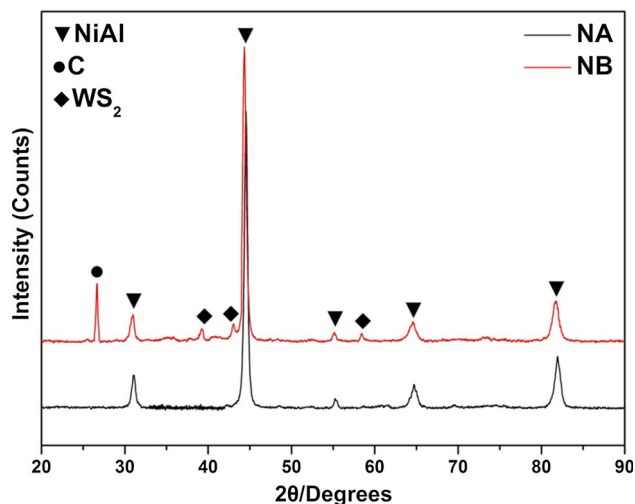


**Fig. 2** XRD patterns of NA and NB

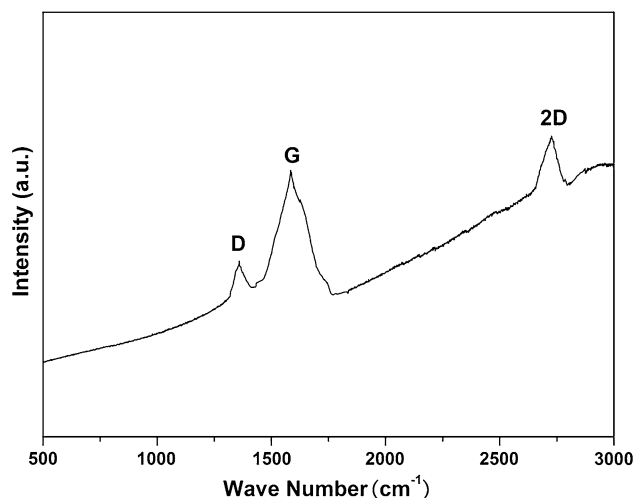


**Fig. 3** The Raman spectra of the surface of NB

phonon mode (E<sub>2g</sub> symmetry) at the Brillouin zone center observed at  $\sim 1,580 \text{ cm}^{-1}$  originating from in-plane vibration of  $sp^2$  carbon atoms; the D mode arising from the doubly resonant disorder-induced mode ( $\sim 1,350 \text{ cm}^{-1}$ ); and the symmetry-allowed 2D overtone mode ( $\sim 2,700 \text{ cm}^{-1}$ ), which are the typical features of thick graphene stacks [18]. Table 1 shows the composition, hardness and density of the composites. It is clear that the addition of  $\text{WS}_2$  and MLG obviously improves the hardness and decreases the density of NASC. Table 2 shows the hardness of worn surface of NA and NB after sliding against different counterface balls. As shown in Table 2, the strength of composites is obviously improved after sliding test. It indicates that work hardening can be produced on the worn surface during sliding process.

**Table 1** The composition, hardness and density of the composites

| Sample | Composition (wt%)            | Microhardness (GPa) | Density ( $\text{g mm}^{-3}$ ) |
|--------|------------------------------|---------------------|--------------------------------|
| NA     | NiAl                         | 5.61                | 5.71                           |
| NB     | NiAl–1.5 MLG–5 $\text{WS}_2$ | 6.87                | 5.42                           |

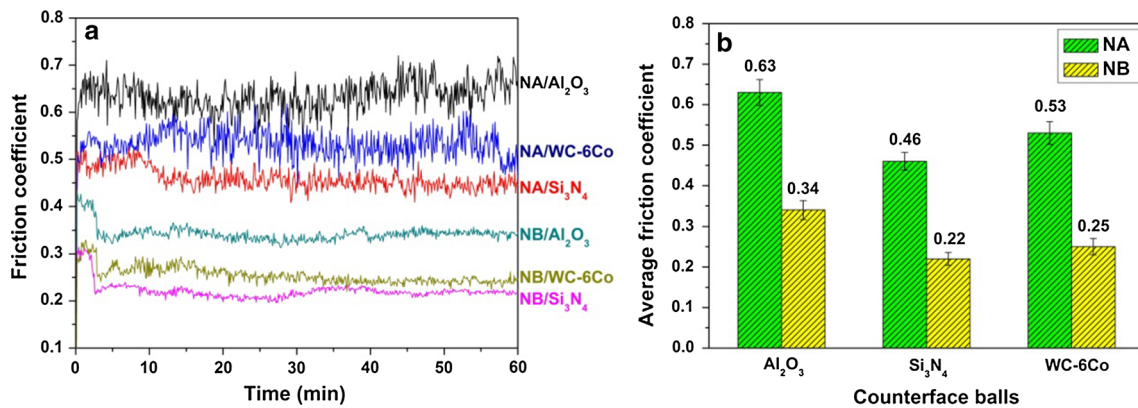
**Table 2** The hardness of worn surface of NA and NB after sliding against different counterface balls

| Sample | Counterface ball        | Microhardness (GPa) |
|--------|-------------------------|---------------------|
| NA     | $\text{Al}_2\text{O}_3$ | 6.63                |
| NA     | $\text{Si}_3\text{N}_4$ | 6.02                |
| NA     | WC–6Co                  | 6.45                |
| NB     | $\text{Al}_2\text{O}_3$ | 8.69                |
| NB     | $\text{Si}_3\text{N}_4$ | 8.12                |
| NB     | WC–6Co                  | 8.43                |

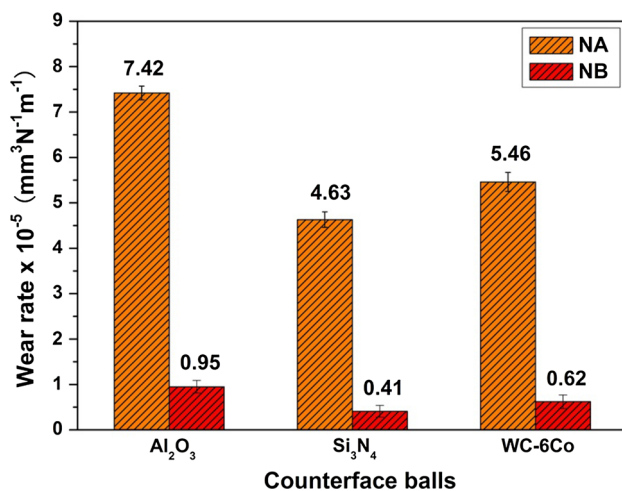
### 3.2 Friction and Wear Behaviors

Figure 4a shows the friction coefficient curves of NA and NB sliding against various balls under a normal load of 10 N and a sliding velocity of  $0.2 \text{ m s}^{-1}$ . Figure 4b shows the average friction coefficients. The error bars are the standard deviations of the average friction coefficients. It is clear that the friction coefficients of NB for all the three types of counterface balls are apparently lower than those of NA. As can be seen from Fig. 4b, the friction coefficient is observed to decrease from 0.63 to 0.34 when sliding against  $\text{Al}_2\text{O}_3$ , from 0.46 to 0.22 when sliding against  $\text{Si}_3\text{N}_4$  and from 0.53 to 0.25 when sliding against WC–6Co by the addition of  $\text{WS}_2$  and MLG. Besides, NA and NB have the highest friction coefficients when sliding against  $\text{Al}_2\text{O}_3$ , while NA and NB have the lowest friction coefficients when sliding against  $\text{Si}_3\text{N}_4$ . It shows that the friction coefficients of NA and NB are closely related to the counterface materials, and the addition of  $\text{WS}_2$  and MLG does not change the optimum counterface of NiAl composites. Moreover, it can be found that the friction coefficient curves of NB become relatively stable for all the three types of counterface balls after a short period of running-in. It may be attributed to the formation of lubricating films under the action of continuous extrusion stress and cyclic shear stress during early stages of sliding friction.

Figure 5 shows the wear rates of NA and NB sliding against various balls under a normal load of 10 N and a sliding velocity of  $0.2 \text{ m s}^{-1}$ . The error bars are the standard deviations of the average wear rates. It is clear that the wear rates of NB for all the three types of counterface balls are apparently lower than those of NA. As can be seen from Fig. 5, the wear rate is observed to decrease from



**Fig. 4** **a** The friction coefficient curves of NA and NB sliding against various balls; **b** the average friction coefficients



**Fig. 5** The wear rates of NA and NB sliding against various balls

$7.42 \times 10^{-5}$  to  $0.95 \times 10^{-5}$  mm<sup>3</sup> N<sup>-1</sup> m<sup>-1</sup> when sliding against Al<sub>2</sub>O<sub>3</sub>, from  $4.63 \times 10^{-5}$  to  $0.41 \times 10^{-5}$  mm<sup>3</sup> N<sup>-1</sup> m<sup>-1</sup> when sliding against Si<sub>3</sub>N<sub>4</sub> and from  $5.46 \times 10^{-5}$  to  $0.62 \times 10^{-5}$  mm<sup>3</sup> N<sup>-1</sup> m<sup>-1</sup> when sliding against WC-6Co by the addition of WS<sub>2</sub> and MLG. Besides, the counterface materials have a strong influence on the wear rates of NA and NB. As can be seen from Fig. 5, NA and NB sliding against Al<sub>2</sub>O<sub>3</sub> result in the largest wear rate, while they sliding against Si<sub>3</sub>N<sub>4</sub> result in the lowest wear rate.

Figure 6 shows the wear rates of counterface balls. The error bars are the standard deviations of the average wear rates. The friction wears of counterface balls are a little due to their higher hardness in respect to NA and NB (shown in Table 1). It can be found that the wear rates for all the three types of counterface balls decrease when sliding against NB. It may be also attributed to the formation of lubricating films during the sliding process. The wear rates of Al<sub>2</sub>O<sub>3</sub> balls are the largest, which are  $1.32 \times 10^{-5}$  and  $0.4 \times 10^{-5}$  mm<sup>3</sup> N<sup>-1</sup> m<sup>-1</sup>, respectively. The wear rates of

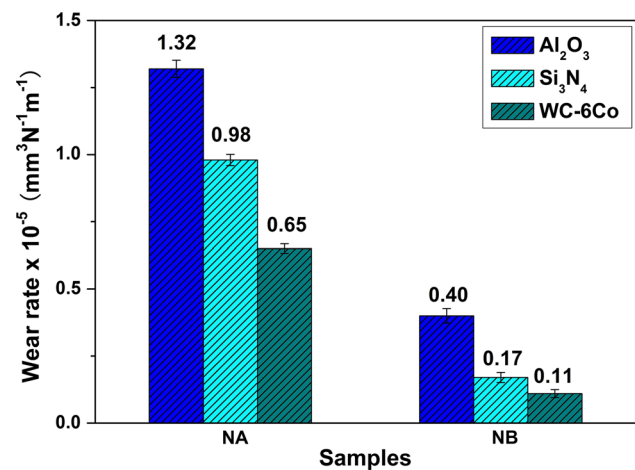


**Fig. 6** The wear rates of counterface balls

WC-6Co balls are the lowest, which are  $0.65 \times 10^{-5}$  and  $0.11 \times 10^{-5}$  mm<sup>3</sup> N<sup>-1</sup> m<sup>-1</sup>, respectively.

The results above show that the tribological properties of NiAl composites are obviously improved through adding WS<sub>2</sub> and MLG solid lubricants. Moreover, the tribological properties of NASC are closely related to the counterface materials.

### 3.3 Wear and Lubrication Mechanisms

The friction coefficient and wear rate of NiAl composites are significantly reduced by the addition of WS<sub>2</sub> and MLG. In order to understand the wear and lubrication mechanisms involved in the different contact pairs, EPMA is used to examine the morphologies of worn surfaces of NA and NB with different counterface balls. EDS is used to analyze the compositions of the worn surfaces. The discussion in this paper focuses on the tribological properties of NASC; the wear mechanism of the counterface balls will not be analyzed.

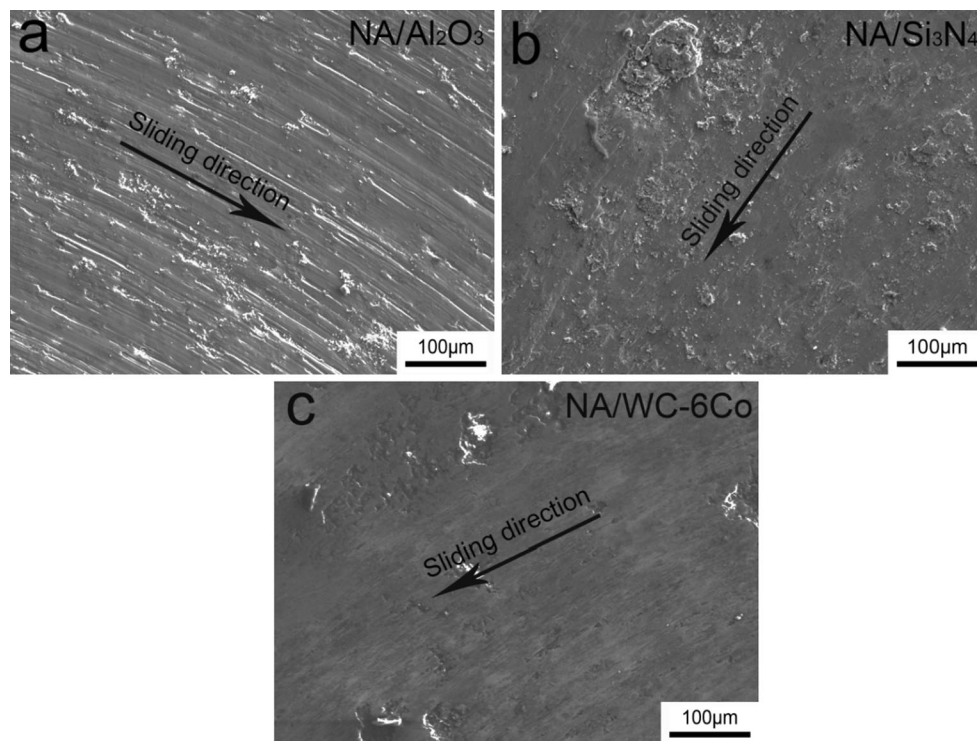


**Fig. 7** The wear track morphologies of NA after sliding against various balls

Figure 7 shows the wear track morphologies of NA after sliding against various balls. As shown in Fig. 7a, NA exhibits a rough worn surface, which is characterized by deep parallel distributed grooves along the sliding direction of the  $\text{Al}_2\text{O}_3$  ball. The hardness of  $\text{Al}_2\text{O}_3$  ball is much higher than NA. During the sliding friction process, the hard protrusions on the  $\text{Al}_2\text{O}_3$  ball penetrate into the softer surface of NA and remove the materials of NA by micro-cutting and plowing. The grooves on the surface of NA undoubtedly suggest that the main wear mechanism is abrasive wear. As shown in Fig. 7b, some slight scratches and a considerable amount of agglomerated wear debris can be observed on the surface of NA after sliding against  $\text{Si}_3\text{N}_4$  ball. The wear debris particles contain Ni and Al elements, as well as Si and O elements as suggested by the EDS analysis. The wear track morphology suggests that large amount of wear debris of Ni–Al–Si oxides are generated during sliding friction process and some wear debris stick to the wear surface under the applied contact pressure. The layer of wear debris may play a role of lubrication and thus results in a lower friction coefficient between the friction pair of NA/ $\text{Si}_3\text{N}_4$  than those between other friction pairs. Therefore, the main wear mechanisms of NA in the friction pair of NA/ $\text{Si}_3\text{N}_4$  are abrasion wear and adhesive wear. As shown in Fig. 7c, the plastic flow traces and some fracture spots in the form of craters can be seen on the wear

track of NA in the friction pair of NA/WC–6Co. It implies that plastic deformation and abrasion as the main wear mechanisms dominate the wear process of NA while the counterface is WC–6Co ball. However, the wear track morphologies of NA in Fig. 7 show that the worn surface of NA in the friction pair of NA/WC–6Co is relatively smoother than those in the other friction pairs. Deep grooves or large amount of wear debris cannot be observed on the worn surface of NA in the friction pair of NA/WC–6Co. Such difference in wear track morphologies of NA sliding against various balls can be explained by the wear volume loss of different counterface balls. As shown in Fig. 6, WC–6Co ball has lower wear rate than  $\text{Al}_2\text{O}_3$  and  $\text{Si}_3\text{N}_4$  after sliding against NA. It can be predicted that the hard particles of WC–6Co in the wear debris are less in quantity, and the geometry of the particles is less aggressive. Hence, abrasive wear of NA in the friction pair of NA/WC–6Co is less intensity than those in the other two friction pairs of NA/ $\text{Al}_2\text{O}_3$  and NA/ $\text{Si}_3\text{N}_4$ .

Figure 8 shows the wear track morphologies of NB after sliding against various balls. The wear track morphologies of NB clearly indicate that the worn surface is covered with a continuous lubricating film in all the cases [12, 29]. The EDS analysis results of the areas marked by rectangles on the worn surfaces of NB shown in Fig. 8 are given in Table 3. As shown in Fig. 8a, NB has a comparative

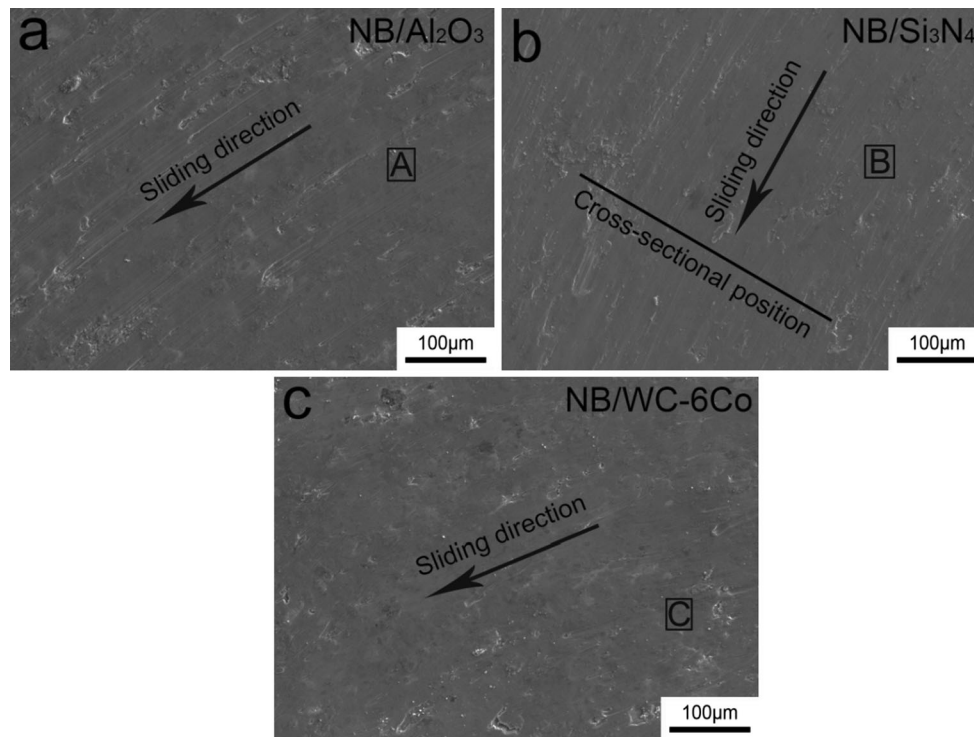


**Fig. 8** The wear track morphologies of NB after sliding against various balls

smoother worn surface than NA after sliding against  $\text{Al}_2\text{O}_3$  ball, but parallel distributed scratches and fracture spots can also be seen on the worn surface of NB. It implies that abrasive wear still dominates the wear process of NB, while the counterface is  $\text{Al}_2\text{O}_3$  ball. However, a continuous lubricating film is formed on the worn surface and decreases the intensity of micro-cutting and plowing commonly encountered in abrasive wear [1]. The EDS analysis result of area A on the worn surfaces of NB in the friction pair of NB/ $\text{Al}_2\text{O}_3$  shows that the continuous lubricating film contains abundant W, S and C elements. It indicates that  $\text{WS}_2$  and MLG can be provided to the worn surface to form a lubricating film under the action of continuous extrusion stress and cyclic shear stress. The lubricating film provides the low-strength junctions at the interface, reducing the friction coefficient and wear rate during dry friction process. As shown in Fig. 8b, the wear track morphology shows a smooth surface covered by a continuous lubricating film. Some slight scratches and loose fine wear debris suggest that the wear mechanism is dominated by abrasive wear. The smooth and well-compacted film contains abundant W, S and C elements as suggested by the EDS analysis. The low friction coefficient and wear rate of NB in the friction pair of NB/ $\text{Si}_3\text{N}_4$  may be attributed to the lubricating effect of the  $\text{WS}_2$  and MLG. The protective lubricating film provides the low-strength junctions and reduces the contact between NiAl matrix and

**Table 3** The EDS analysis results (wt%) of the areas marked by rectangles on the worn surfaces of NB

| Area | C    | O    | Al    | S    | Ni    | Mo   | W    | Nb   |
|------|------|------|-------|------|-------|------|------|------|
| A    | 2.01 | 7.87 | 25.15 | 2.26 | 52.09 | 2.13 | 6.42 | 2.07 |
| B    | 2.32 | 3.48 | 27.23 | 2.50 | 54.76 | 1.04 | 7.11 | 1.56 |
| C    | 3.98 | 5.09 | 24.97 | 2.47 | 49.84 | 1.87 | 9.13 | 2.65 |

$\text{Si}_3\text{N}_4$  ball, then effectively reducing the generation of wear debris. As shown in Figs. 7b and 8b, it can be found that fewer wear debris are produced in the friction pair of NB/ $\text{Si}_3\text{N}_4$  than in the friction pair of NA/ $\text{Si}_3\text{N}_4$ . As shown in Fig. 8c, some slight scratches and fracture spots in the form of craters can be seen on the wear track of NB in the friction pair of NB/WC–6Co. The wear mechanism is characterized by abrasive wear. The EDS analysis result of area C on the worn surfaces of NB in the friction pair of NB/WC–6Co shows that the continuous glaze film contains abundant W, S and C elements. It indicates that  $\text{WS}_2$  and MLG can also diffuse to the sliding surface under the action of continuous extrusion stress and cyclic shear stress and form low shearing stress junctions, lowering the friction coefficient and wear rate. Moreover, no obvious plastic flow traces can be observed on the worn surface of NB in the friction pair of NB/WC–6Co. It may be owing to the fact that the lubricating film containing abundant  $\text{WS}_2$  and

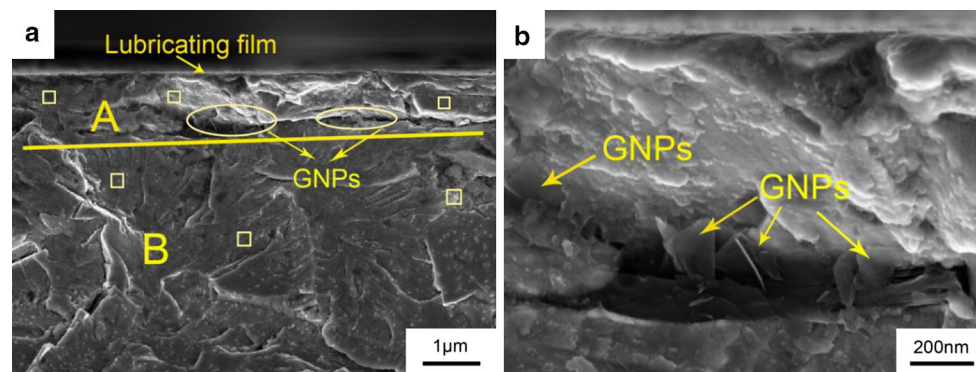


**Fig. 9** **a** A FESEM image of the cross-section of the wear track of NB; **b** the high-magnification images for *layer A* in **a**

**Table 4** The mean values (wt%) of EDS analysis for all elements of different layers

| Layer | C    | O    | Al    | S    | Ni    | Mo   | W    | Nb   |
|-------|------|------|-------|------|-------|------|------|------|
| A     | 2.38 | 3.12 | 25.84 | 2.61 | 53.89 | 2.36 | 7.49 | 2.31 |
| B     | 1.26 | –    | 29.35 | 1.09 | 61.03 | 2.14 | 3.11 | 2.02 |

MLG is capable of playing a role of lubricant which increases the capacity for resisting plastic deformation in sliding process.

In general, NB shows better self-lubricity than NA in all the cases. Solid lubricants of  $WS_2$  and MLG can be provided to the worn surface of NB to form a smooth and well-compacted lubricating film while NB sliding against different materials of counterface balls. However, abrasive wear is the main wear mechanism of NA and NB in all the friction pairs. The reason can be explained based on the fact that the balls made of  $Al_2O_3$ ,  $Si_3N_4$  and WC–6Co have a considerably higher hardness than NA and NB, even if strong working hardness effect is developed on the worn surface during sliding process.

The above results suggest that the wear and lubrication mechanisms of NB in the three different friction pairs are similar. NB exhibits excellent self-lubricating properties by forming a lubricating layer while sliding against  $Al_2O_3$ ,  $Si_3N_4$  or WC–6Co balls. In order to investigate the forming mechanism of lubricating layer on the worn surface of NB during the sliding friction process, the friction pair of NB/ $Si_3N_4$  is chosen for further analysis. It has been well known that the basic factor of determining the forming mechanism of lubricating layer will be the subsurface deformation, which changes the microstructure and properties of subsurface materials [30]. Herein, the investigation of microstructure evolution underneath the worn surface is quite significant in revealing the anti-wear and friction-reducing mechanisms of the solid lubricants in matrix material. The subsurface analysis is carried out on the surface by cross-sectioning it perpendicular to the sliding direction, and the

location of the cross-sectional position is shown in Fig. 8b. The typical FESEM micrographs underneath the wear track of NB after sliding against  $Si_3N_4$  ball are shown in Fig. 9. Figure 9a is a FESEM image of the cross-section of the wear track of NB. As shown in Fig. 9a, the significant stratification morphology along the depth is easily identified and two distinct regions are marked A and B. The high-magnification FESEM image for layer A in Fig. 9a is shown in Fig. 9b. The image shown in Fig. 9b presents that the MLG still persists in the NiAl matrix and a large amount of MLG accumulates in layer A during the sliding process. The MLG helps transfer the load from NiAl matrix and prevents crack propagation, which would increase the fracture toughness of NiAl matrix. Similar reinforced mechanisms have been also reported by others researchers [17]. In order to accurately determine the elemental compositions, elements in three areas marked by rectangles of each layer as shown in Fig. 9a are analyzed by EDS method. The mean values of three measurements for all elements are given in Table 4. Table 4 shows that layer A contains W and S elements in large quantity. The Raman spectra of the worn surface of NB are shown in Fig. 10. As shown in Fig. 10, the Raman spectra of the worn surface of NB present alike characteristics with D, G and 2D peaks, which are the typical features of thick graphene stacks [18]. It implies that MLG is indeed present within the sliding wear track area. MLG has the low shear and highly protective nature as mentioned in Ref. [31]. It can reduce wear and friction on sliding surface. Moreover, the EBSD image of the subsurface under the worn surface of NB when sliding against  $Si_3N_4$  is shown in Fig. 11. It shows the results of the phase distribution with the NiAl phase marked in red, MLG phase marked in yellow and  $WS_2$  phase marked in green. Clearly, MLG and  $WS_2$  accumulate in the region near the worn surface. It can be concluded that  $WS_2$  and MLG, which are added as the lubricants, overcome the potential barrier and diffuse to the sliding surface in the process of sliding wear. MLG in layer A



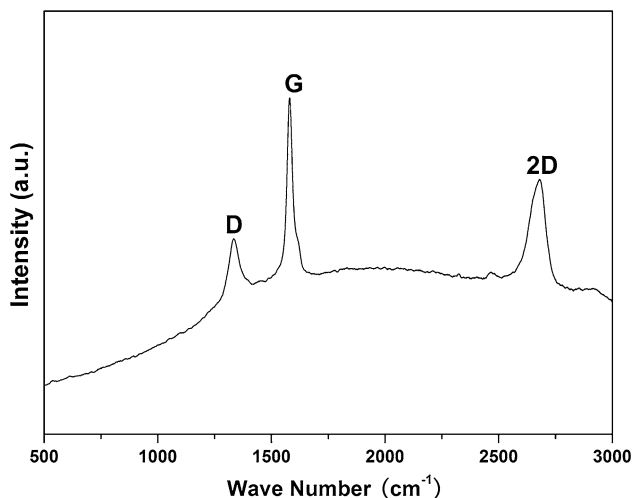


**Fig. 10** The Raman spectra of the worn surface of NB

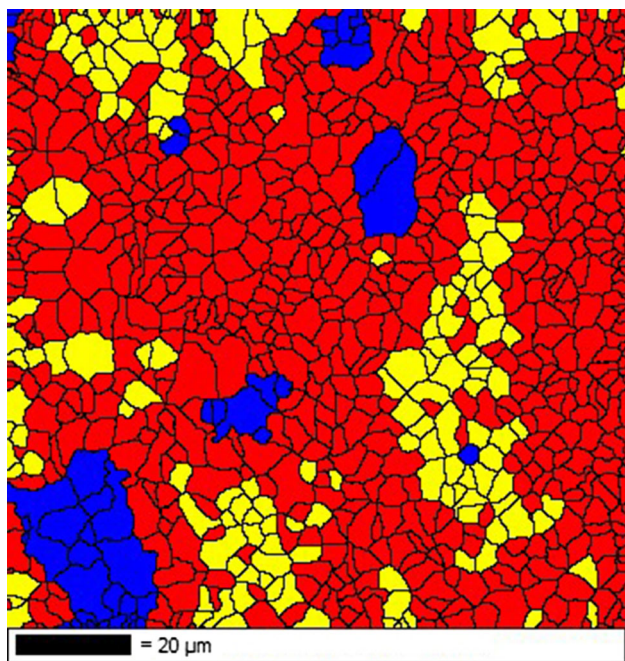


**Fig. 11** EBSD image of the subsurface under the worn surface of NB when sliding against  $\text{Si}_3\text{N}_4$  (the phase distribution with the NiAl phase marked in red, MLG phase marked in yellow and  $\text{WS}_2$  phase marked in green) (Color figure online)

increases the capacity for resisting deformation and enhances the fracture toughness and flexural strength of the composite. Hence, it is hard to remove materials from worn surface during the process of abrasive wear, and abrasive wear of NB is less intensity when  $\text{WS}_2$  and MLG are highly concentrated in layer A. Under the action of continuous extrusion stress and due to the circular sliding of  $\text{Si}_3\text{N}_4$

counterface ball on the same wear track, a continuous lubricating film is formed on the upmost surface of layer A. The lubricating film provides the low-strength junctions at the interface, significantly reducing the friction coefficient and wear rate during the sliding process.

#### 4 Conclusion

In this article, MLG and  $\text{WS}_2$  were used as solid lubricants to design NASC. Tribological behaviors of the as-prepared composites were investigated by sliding against counterface balls made of  $\text{Al}_2\text{O}_3$ ,  $\text{Si}_3\text{N}_4$  and WC–6Co. The results showed that the tribological properties of NiAl composites were obviously improved after adding  $\text{WS}_2$  and MLG. Besides, the counterface materials had a strong influence on the friction coefficients and wear rates of NA and NB. Moreover, the counterface balls sliding against NB had lower wear rates than those sliding against NA. The wear track morphologies of NA and NB exhibited that abrasive wear was the main wear mechanism of NA and NB in all the friction pairs. It was attributed to the fact that the balls made of  $\text{Al}_2\text{O}_3$ ,  $\text{Si}_3\text{N}_4$  and WC–6Co had a considerably higher hardness than NA and NB, even if strong work hardening effect was developed on the worn surface during sliding process.

The subsurface analysis showed that a layer A containing abundant  $\text{WS}_2$  and MLG was formed due to the deformation and flow of  $\text{WS}_2$  and MLG in the process of sliding wear. MLG in layer A provided better capacity to resist deformation and increased the fracture toughness and flexural strength of the composite. During the sliding process, layer A helped transfer the load from the NiAl matrix and reduced the material removal. Moreover, a continuous lubricating film was formed on the upmost surface of layer A. The lubricating film provided the low-strength junctions at the interface, further reducing the friction coefficient and wear rate of NB. The addition of a combination of  $\text{WS}_2$  and MLG offered an opportunity to prepare NASC that possessed superior antifriction and wear resistance. In addition, the present work provided valuable information that the potential of MLG used as solid lubricant, providing combined lubrication with other solid lubricants.

**Acknowledgments** This work was supported by the National Natural Science Foundation of China (51275370); the Nature Science Foundation of Hubei Province (2012FFB05104); the Fundamental Research Funds for the Central Universities (2014-yb-004); the Project for Science and Technology Plan of Wuhan City (2013010501010139); the Academic Leader Program of Wuhan City (201150530146); and the Project for Teaching and Research project of Wuhan University of Technology (2012016). The authors also wish to gratefully thank the Material Research and Testing Center of Wuhan University of Technology for their assistance.

## References

- Tyagi, R., Xiong, D.S., Li, J.L., Dai, J.H.: Elevated temperature tribological behavior of NiAl based composites containing nano-silver and hBN. *Wear* **269**, 884–890 (2010)
- Wu, Y., Wang, F., Cheng, Y., Chen, N.: A study of the optimization mechanism of solid lubricant concentration in NiMoS<sub>2</sub> self-lubricating composite. *Wear* **205**, 64–70 (1997)
- Evans, D.C., Senior, G.S.: Self-lubricating materials for plain bearings. *Tribol. Int.* **15**, 243–248 (1982)
- Xiong, D.S.: Lubrication behavior of Ni–Cr-based alloys containing MoS<sub>2</sub> at high temperature. *Wear* **251**, 1094–1099 (2001)
- Zhu, S.Y., Bi, Q.L., Yang, J., Liu, W.M.: Tribological property of Ni<sub>3</sub>Al matrix composites with addition of BaMoO<sub>4</sub>. *Tribol. Lett.* **43**, 55–63 (2011)
- Fan, X.M., Yin, X.W., He, S.S., Zhang, L.T., Cheng, L.F.: Friction and wear behaviors of C/C–SiC composites containing Ti<sub>3</sub>SiC<sub>2</sub>. *Wear* **274–275**, 188–195 (2012)
- Shi, X.L., Xu, Z.S., Wang, M., Zhai, W.Z., Yao, J., Song, S.Y., Abid, Q.D., Zhang, Q.X.: Tribological behavior of TiAl matrix self-lubricating composites containing silver from 25 to 800°C. *Wear* **303**, 486–494 (2013)
- Darolia, R.: NiAl alloys for high-temperature structural applications. *JOM* **43**, 44–49 (1991)
- Noebe, R.D., Bowman, P.R., Nathal, M.V.: Review of the physical and mechanical properties of the B<sub>2</sub> compound NiAl. *Int. Mater. Rev.* **38**, 193–232 (1993)
- Johnson, B.J., Kennedy, F.E., Baker, I.: Dry sliding wear of NiAl. *Wear* **192**, 241–247 (1996)
- Ozdemir, O., Zeytin, S., Bindal, C.: Tribological properties of NiAl produced by pressure-assisted combustion synthesis. *Wear* **265**, 979–985 (2008)
- Zhu, S.Y., Bi, Q.L., Niu, M.Y., Yang, J., Liu, W.M.: Tribological behavior of NiAl matrix composites with addition of oxides at high temperatures. *Wear* **274–275**, 423–434 (2012)
- Murakami, T., Ouyang, J.H., Sasaki, S., Umeda, K., Yoneyama, Y.: High-temperature tribological properties of Al<sub>2</sub>O<sub>3</sub>, Ni–20mass%Cr and NiAl spark-plasma-sintered composites containing BaF<sub>2</sub>–CaF<sub>2</sub> phase. *Wear* **259**, 626–633 (2005)
- Shi, X.L., Zhai, W.Z., Xu, Z.S., Wang, M., Yao, J., Song, S.Y., Wang, Y.F.: Synergetic lubricating effect of MoS<sub>2</sub> and Ti<sub>3</sub>SiC<sub>2</sub> on tribological properties of NiAl matrix self-lubricating composites over a wide temperature range. *Mater. Des.* **55**, 93–103 (2014)
- Lee, C., Wei, X.D., Kysar, J.W., Hone, J.: Measurement of the elastic properties and intrinsic strength of monolayer graphene. *Science* **321**, 385–388 (2008)
- Lin, L.Y., Kin, D.E., Kim, W.K., Jun, S.C.: Friction and wear characteristics of multi-layer graphene film investigated by atomic force microscopy. *Surf. Coat. Technol.* **205**, 4864–4869 (2011)
- Kvetkova, L., Duszova, A., Hvizdos, P., Dusza, J., Kun, P., Balazsi, C.: Fracture toughness and toughening mechanisms in graphene platelet reinforced Si<sub>3</sub>N<sub>4</sub> composites. *Scr. Mater.* **66**, 7793–7796 (2012)
- Xu, Z.S., Shi, X.L., Zhai, W.Z., Yao, J., Song, S.Y., Zhang, Q.X.: Preparation and tribological properties of TiAl matrix composites reinforced by multilayer graphene. *Carbon* **67**, 168–177 (2014)
- Deng, J.X., Cao, T.K.: Self-lubricating mechanisms via the in situ formed tribofilm of sintered ceramics with CaF<sub>2</sub> additions when sliding against hardened steel. *Int. J. Refract. Met. Hard Mater.* **25**, 189–197 (2007)
- Kandanur, S.S., Rficee, M.A., Yavari, F., Schrameyer, M., Yu, Z.Z., Blanchet, T.A., Koratkar, N.: Suppression of wear in graphene polymer composites. *Carbon* **50**, 3178–3183 (2012)
- Chhowalla, M., Amaratunga, G.A.J.: Thin films of fullerene-like MoS<sub>2</sub> nanoparticles with ultra-low friction and wear. *Nature* **407**, 164–167 (2000)
- Yang, M.S., Liu, X.B., Fan, J.W., He, X.M., Shi, S.H., Fu, G.Y., Wang, M.D., Chen, S.F.: Microstructure and wear behaviors of laser clad NiCr/Cr<sub>3</sub>C<sub>2</sub>–WS<sub>2</sub> high temperature self-lubricating wear-resistant composite coating. *Appl. Surf. Sci.* **258**, 3757–3762 (2012)
- Zhu, Q.S., Shi, X.L., Zhai, W.Z., Yao, J., Ibrahim, A.M.M., Xu, Z.S., Song, S.Y., Abid, Q.D., Chen, L., Xiao, Y.C., Zhang, Q.X.: Effect of counterface balls on friction layer of Ni<sub>3</sub>Al matrix composites with 1.5 wt% graphene nanoplatelets. *Tribol. Lett.* **55**, 343–352 (2014)
- Shi, X.L., Song, S.X., Zhai, W.Z., Wang, M., Xu, Z.S., Yao, J., Abid, Q.D., Zhang, Q.X.: Tribological behavior of Ni<sub>3</sub>Al matrix self-lubricating composites containing WS<sub>2</sub>, Ag and hBN tested from room temperature to 800°C. *Mater. Des.* **55**, 75–84 (2014)
- American Society for Testing and Materials, Standard test method for Knoop and Vickers hardness of metallic materials, ASTM E384-11e1 (2012)
- American Society for Testing and Materials. Standard test methods for density of compacted or sintered powder metallurgy (PM) products using Archimedes’ principle, ASTM B962-13 (2013)
- American Society for Testing and Materials, Standard test method for wear testing with a pin-on-disk apparatus, ASTM G99-05 (2005)
- Li, C.X., Xia, J., Dong, H.: Sliding wear of TiAl intermetallics against steel and ceramics of Al<sub>2</sub>O<sub>3</sub>, Si<sub>3</sub>N<sub>4</sub> and WC/Co. *Wear* **261**, 693–701 (2006)
- Pauschitz, A., Roy, M., Franek, F.: Mechanisms of sliding wear of metals and alloys at elevated temperatures. *Tribol. Int.* **41**, 584–602 (2008)
- Kolubaev, A., Tarasov, S., Sizova, O., Kolubaev, E.: Scale-dependent subsurface deformation of metallic materials in sliding. *Tribol. Int.* **43**, 695–699 (2010)
- Berman, D., Erdemir, A., Sumant, A.V.: Few layer graphene to reduce wear and friction on sliding steel surfaces. *Carbon* **54**, 454–459 (2013)